Angela Bonaccorso

INFN PISA
Istituto Nazionale di Fisica Nucleare
Sezione di Pisa

Meeting dell'iniziativa specifica MONSTRE
May 11, 2023, 2:00 PM → May 12, 2023, 5:00 PM Europe/Rome
Milano

Exotic nuclei and phenomenological optical potentials

^{9}Be, ^{12}C

In collaboration with Imane Moumene, GGI, Firenze,
now at Milano University.

Motivations to fit optical potentials

The Optical Potential (OP) is obtained from the reduction of the many body scattering problem to a one body Schrödinger equation

- A good OP can give useful information on the structure of a nucleus besides helping describing complex reactions.
- Phenomenological vs *microscopic* OP.
- ^{9}Be
- ^{12}C
- ^{12}C+^{12}C as a test
- ^{12}C+^{9}Be
- ^{12}C and ^{9}Be are the most used targets for nuclear breakup (knockout) with RIBs

Motivations to calculate reaction cross section

- An immediate test for the accuracy of the imaginary part of the potential. Plenty of data to compare to.
- Realistic nuclear reaction cross-section (σ_R) models are an essential ingredient of reliable heavy-ion transport codes. Such codes are used for risk evaluation of manned space exploration missions as well as for ion-beam therapy dose calculations and treatment planning (M. Fukuda et al.)
- From the beginning of physics with RIBs comparison of measured and calculated σ_R has been applied to deduce density distributions of exotic nuclei as well as their root mean square radii (rms). (Tanihata et al., Y. Suzuki et al….)
- Finally the core-target survival probability in knockout reactions can be fixed by reproducing σ_R.
- **Predictive power of models**?

A. Bonaccorso, D.Ph. thesis, Oxford 1980,

"A microscopic theory of the alpha-nucleus optical potential"

https://ora.ox.ac.uk/objects/uuid:d77df433-a09d-46c2-b94b-4d032fcf39b4

PHYSICAL REVIEW C VOLUME 22, NUMBER 3 SEPTEMBER 1980

Nucleus-nucleus total reaction cross sections

R. M. DeVries and J. C. Peng

PHYSICAL REVIEW C VOLUME 35, NUMBER 5 MAY 1987

Trends of total reaction cross sections for heavy ion collisions in the intermediate energy range

S. Kox,[a] A. Gamp,*[a],[b] C. Perrin,[a] J. Arvieux,†[a] R. Bertholet,[c] J. F. Bruandet,[a] M. Buenerd,[a] R. Cherkaoui,‡[a] A. J. Cole,[a] Y. El-Masri,[a],[d] N. Longequeue,[a] J. Menet,[a] F. Merchez,[a] and J. B. Viano[a]

Physics Letters B 268 (1991) 339–344
North-Holland

PHYSICS LETTERS B

Neutron halo in ^{11}Be studied via reaction cross sections

M. Fukuda [1], T. Ichihara, N. Inabe, T. Kubo, H. Kumagai, T. Nakagawa, Y. Yano, I. Tanihata
RIKEN, 2-1 Hirosawa, Wako, Saitama 351-01, Japan

M. Adachi, K. Asahi, M. Kouguchi [2]
Department of Applied Physics, TIT, Meguro, Tokyo 152, Japan

M. Ishihara [3], H. Sagawa and S. Shimoura
Department of Physics, University of Tokyo, 7-3-1 Hongo, Bunkyo-ku, Tokyo 113, Japan

Nuclear Physics A543 (1992) 722–750
North-Holland

NUCLEAR PHYSICS A

Glauber model analysis of the fragmentation reaction cross sections of ^{11}Li

Y. Ogawa[a], K. Yabana[b,1] and Y. Suzuki[b]

J. Phys. G: Nucl. Part. Phys. **22** (1996) 157–198. Printed in the UK

TOPICAL REVIEW

Neutron halo nuclei

Isao Tanihata

RIKEN, 2–1 Hirosawa, Wako, Saitama 351–01, Japan

Progress in Particle and Nuclear Physics 97 (2017) 1–52

Contents lists available at ScienceDirect

Progress in Particle and Nuclear Physics

journal homepage: www.elsevier.com/locate/ppnp

Review

Proton elastic scattering from stable and unstable nuclei — Extraction of nuclear densities

H. Sakaguchi [a,*], J. Zenihiro [b]

[a] RCNP, Osaka University, Japan
[b] RIKEN Nishina Center, Japan

PHYSICAL REVIEW C **79**, 061601(R) (2009)

Reaction cross sections at intermediate energies and Fermi-motion effect

M. Takechi,[1,*] M. Fukuda,[1] M. Mihara,[1] K. Tanaka,[2] T. Chinda,[1] T. Matsumasa,[1] M. Nishimoto,[1] R. Matsumiya,[1] Y. Nakashima,[1] H. Matsubara,[1] K. Matsuta,[1] T. Minamisono,[3] T. Ohtsubo,[4] T. Izumikawa,[5] S. Momota,[6] T. Suzuki,[7] T. Yamaguchi,[7] R. Koyama,[4] W. Shinozaki,[4] M. Takahashi,[4] A. Takizawa,[4] T. Matsuyama,[4] S. Nakajima,[7] K. Kobayashi,[7] M. Hosoi,[7] T. Suda,[2] M. Sasaki,[8] S. Sato,[9] M. Kanazawa,[9] and A. Kitagawa[9]

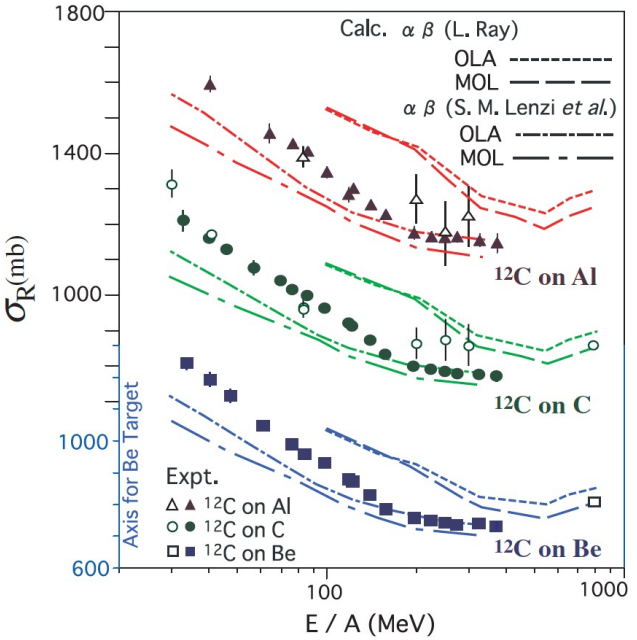

FIG. 1. (Color online) The σ_R data for ^{12}C as a function of beam energy. The closed symbols denote the present data and open symbols denote data from Refs. [8,25–27]. The OLA and MOL calculations were performed using the NN parameters from Ref. [22] (short and long dashed curves) and Ref. [23] (short and long dash-dotted curves).

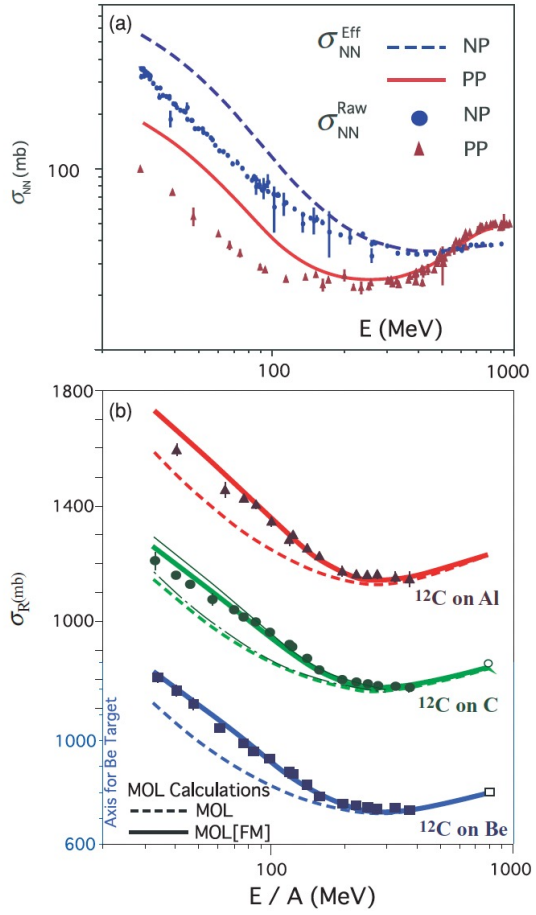

FIG. 2. (Color online) (a) Modified σ_{NN} as effective NN cross section (σ_{NN}^{eff}), which is compared with the raw σ_{NN}. (b) MOL calculations with $\beta(E)$ from Eq. (4) (dashed curve) and MOL[FM] calculations (solid curve) are compared with experimental data. We also show the MOL and MOL[FM] calculations using a Gaussian-type density for the C target (thin solid and dot-dashed curves).

See talks of C. Barbieri, P. Finelli for ab-initio approaches to nN potentials

Nuclear matter density distributions of the neutron-rich ^{6,8}He isotopes from a sum-of-Gaussian analysis of elastic proton scattering data at intermediate energies

X. Liu, P. Egelhof, O. Kiselev, and M. Mutterer
Phys. Rev. C **104**, 034315 – Published 17 September 2021

GSI:
fit parameters of the density distribution

$$\frac{d\sigma}{dt} = \frac{\pi}{k^2}|F_{el}(\mathbf{q})|^2, \qquad (2)$$

with

$$F_{el} = \frac{ik}{2\pi}\int e^{i\mathbf{qb}}\left\{1 - \prod_i^A [1 - \gamma_{pN}(\mathbf{b} - \mathbf{s}_i)]\right\} \times \rho_A(\mathbf{r}_1, \mathbf{r}_2, \ldots, \mathbf{r}_A) d^3\mathbf{r}_1 d^3\mathbf{r}_2 \ldots d^3\mathbf{r}_A d^2\mathbf{b}. \qquad (3)$$

$$\gamma_{pN}(\mathbf{b}) = \frac{1}{2i\pi k}\int e^{-i\mathbf{qb}} f_{pN}(\mathbf{q}) d^2\mathbf{q}.$$

$$f_{pN}(\mathbf{q}) = \frac{ik}{4\pi}\sigma_{pN}(1 - i\epsilon_{pN}) \exp\left(-\frac{\mathbf{q}^2\beta_{pN}}{2}\right).$$

TABLE II. pN scattering amplitude parameters, σ_{pN}, ϵ_{pN}, and β_{pN}, used for the present SOG analysis of elastic p-^{6,8}He scattering.

Reaction	E_{inc} (MeV/u)	σ_{pp} (mb)	σ_{pn} (mb)	ϵ_{pp}	ϵ_{pn}	β_{pN} (fm^2)
p-^{6}He	717	43.5(1.6)	37.4(1.8)	0.094(41)	−0.299(42)	0.183(5)
p-^{8}He	671	41.4(1.5)	36.7(1.6)	0.132(40)	−0.269(42)	0.183(5)

Available online at www.sciencedirect.com
SciVerse ScienceDirect
Nuclear Physics A 875 (2012) 8–28
www.elsevier.com/locate/nuclphysa

Nuclear-matter density distribution in the neutron-rich nuclei ^{12,14}Be from proton elastic scattering in inverse kinematics

S. Ilieva [a,b,*], F. Aksouh [a], G.D. Alkhazov [c], L. Chulkov [d], A.V. Dobrovolsky [c], P. Egelhof [a], H. Geissel [a], M. Gorska [a], A. Inglessi [a,c], R. Kanungo [a,f], A.V. Khanzadeev [c], O.A. Kiselev [a,e], G.A. Korolev [c], X.C. Le [a], Yu.A. Litvinov [a], C. Nociforo [a], D.M. Seliverstov [c], L.O. Sergeev [c], H. Simon [a], V.A. Volkov [d], A.A. Vorobyov [c], H. Weick [a], V.I. Yatsoura [c], A.A. Zhdanov [c]

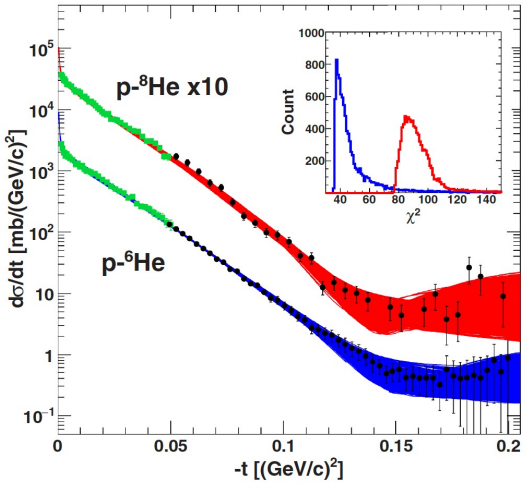

FIG. 4. Measured differential cross sections $d\sigma/dt$ as a function of the four-momentum transfer squared $-t$ for p-^{6}He and p-^{8}He scattering at energies around 700 MeV/u. Green squares represent data measured at low momentum transfer from Ref. [18], and black dots represent data measured at higher momentum transfer from Ref. [27]. The measured differential cross section of p-^{8}He is multiplied by a factor of 10. The bundle of solid lines corresponds to all "good" fits within the framework of the Glauber multiple-scattering theory using SOG distributions for describing the matter densities. The inset shows the probability histograms of the resulting χ^2 values for ^{6}He (in blue) and ^{8}He (in red), respectively.

N+N

The Glauber reaction cross section is given by

$$\sigma_R = 2\pi \int_0^\infty bdb(1 - |S_{NN}(\mathbf{b})|^2), \tag{1}$$

where

$$|S_{NN}(\mathbf{b})|^2 = e^{2\chi_I(b)} \tag{2}$$

is the probability that the nucleus-nucleus (NN) scattering is elastic for a given impact parameter $\mathbf{b}$.

The imaginary part of the eikonal phase shift is given by

$$\chi_I(\mathbf{b}) = \frac{1}{\hbar v}\int dz W^{NN}(\mathbf{b},z)$$
$$= \frac{1}{\hbar v}\int dz \int d\mathbf{r_1} W^{nN}(\mathbf{r_1}-\mathbf{r})\rho(\mathbf{r_1}), \tag{3}$$

where W^{NN} is negative defined as

s.f.

$$W^{NN}(\mathbf{r}) = \int d\mathbf{b_1} W^{nN}(\mathbf{b_1}-\mathbf{b},z)\int dz_1 \rho(\mathbf{b_1},z_1). \tag{4}$$

d.f.

$$W^{NN}(\mathbf{r}) = -\frac{1}{2}\hbar v\sigma_{nn}\int d\mathbf{b_1}\rho_p(\mathbf{b_1}-\mathbf{b},z)\int dz_1\rho_t(\mathbf{b_1},z_1). \tag{5}$$

Also

s.f.

$$W^{nN}(\mathbf{r}) = -\tfrac{1}{2}\hbar v\sigma_{nn}\rho_t(\mathbf{r}) \tag{6}$$

d.f.

$$\chi_I(\mathbf{b}) = -\frac{1}{2}\sigma_{nn}\int d\mathbf{b_1}\int dz\rho_p(\mathbf{b_1}-\mathbf{b},z)\int dz_1\rho_t(\mathbf{b_1},z_1).$$

The double folding (5) for $\mathbf{W^{NN}}$ is conceptually **wrong** because the interaction acts only to first order, infact it was originally introduced for the REAL part. Eq.(4) with a phenomenological W^{nN} is in principle more accurate.

PHYSICAL REVIEW C, VOLUME 62, 034608

Scatterings of complex nuclei in the Glauber model

B. Abu-Ibrahim* and Y. Suzuki

$$e^{i\tilde{\chi}_{\mathrm{OLA}}(b)} = \exp\left(-\int d\boldsymbol{r}\,\rho_P(\boldsymbol{r})\Gamma_{NT}(\boldsymbol{\xi}+\boldsymbol{b})\right),$$

$$\Gamma_{NT}(\boldsymbol{b}) = \sum_{k=1}^{K}\frac{1-i\alpha_k}{4\pi\beta_k}\sigma_k\exp\left(-\frac{\boldsymbol{b}^2}{2\beta_k}\right),$$

Breakup formulae

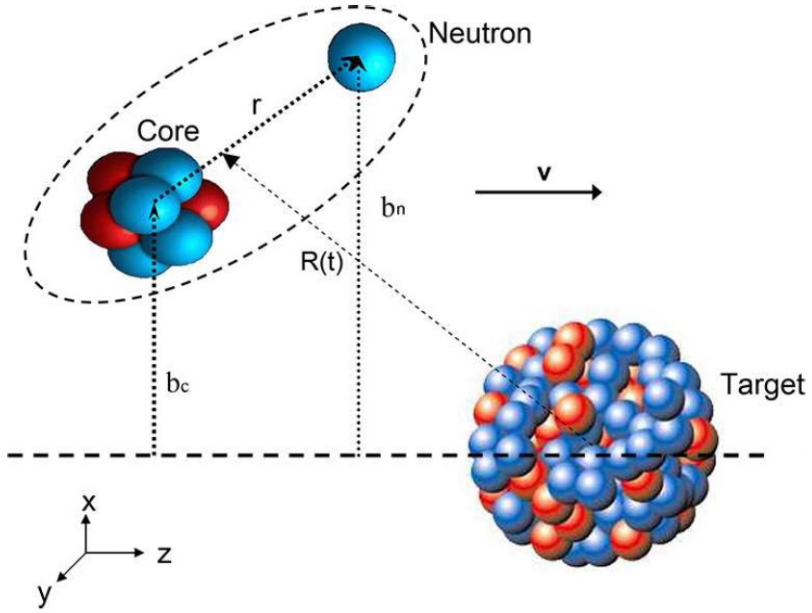

$$\sigma_{-n}^{inel} = \int d^2\mathbf{b_c}|S_{ct}(\mathbf{b_c})|^2 \int d^2\mathbf{r}_\perp(1-|S_n(\mathbf{b_n})|^2)|\tilde{\phi}_0(\mathbf{r}_\perp)|^2$$

$$\sigma_{-n}^{el} = \int \mathrm{d}^2\mathbf{b}_c|S_{ct}\left(\mathbf{b}_c\right)|^2 \int \mathrm{d}^2\mathbf{r}_\perp\,|1-S_n\left(\mathbf{b}_n\right)|^2\,|\tilde{\phi}_0\left(\mathbf{r}_\perp\right)|^2.$$

$R_S = r_S (A_P^{1/3} + A_T^{1/3})$ strong absorption radius

$|S(Rs)|^2 = 1/2$

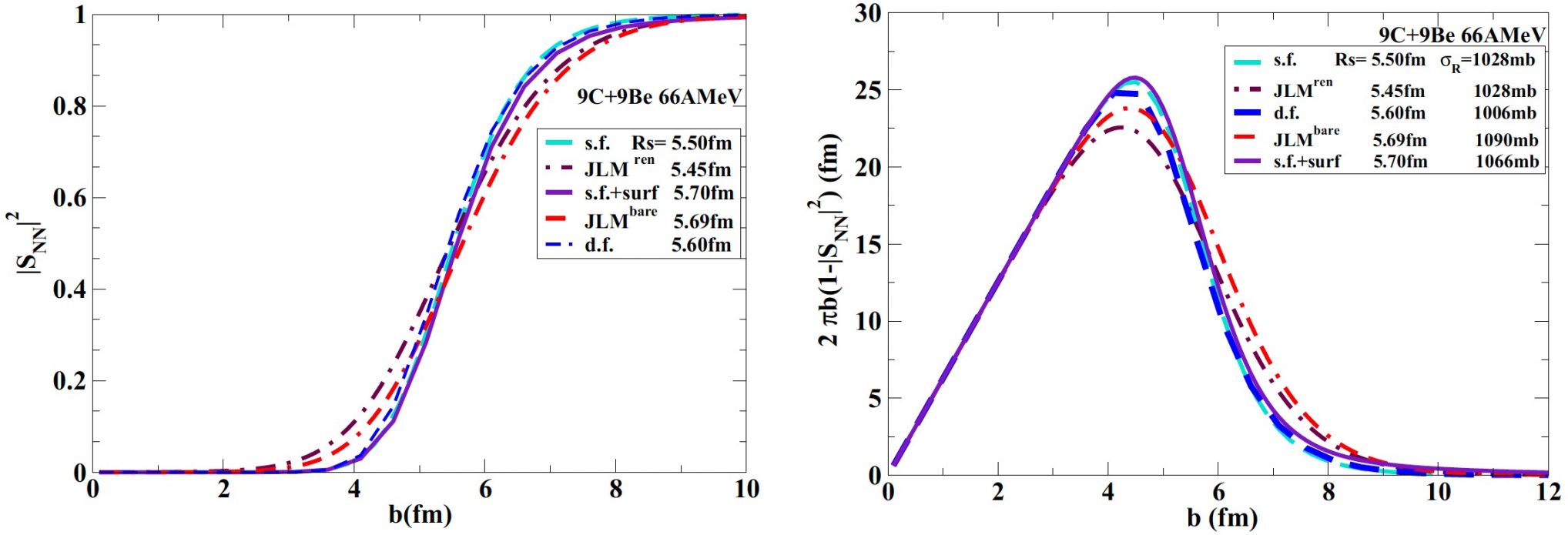

FIG. 5. (LHS) *S* matrices calculated at 66 MeV/nucleon with the potentials indicated in the legend. (RHS) Integrand in Eq. (1). See text for details.

Phenomenological potentials

E_{lab} (MeV)	V^R (MeV)	r_0^R (fm)	a^R (fm)	W^{sur} (MeV)	W^{vol} (MeV)
$20 \leq E_{lab} < 40$	$31.304 - 0.145E_{lab}$	$1.647 - 0.005(E_{lab} - 5)$	$0.3\text{-}0.0001E_{lab}$	$1.65 + 0.365E_{lab}$	$5.6 - 0.005(E_{lab} - 20)$
$40 \leq E_{lab} < 111$	"	"	"	$16.25 - 0.05(E_{lab} - 40)$	$5.5 - 0.01(E_{lab} - 40)$
$111 \leq E_{lab} < 160$	"	"	0.288	12.7	4.8
$160 \leq E_{lab} < 200$	"	"	"	$12.7 - 0.025(E_{lab} - 160)$	$4.8 - 0.025(E_{lab} - 160)$
$200 \leq E_{lab} < 215$	"	"	"	$11.7 + 0.02(E_{lab} - 200)$	$3.8 + 0.02(E_{lab} - 200)$
$215 \leq E_{lab} \leq 500$	0	"	"	"	"

TABLE I: Energy-dependent optical-model parameters for the (AB) potential for n+^{9}Be. r_0^I=1.3 fm, a^I=0.3 fm at all energies.

E_{lab} (MeV)	V^R (MeV)	r_0^R (fm)	a^R (fm)	W^{sur} (MeV)	W^{vol} (MeV)
$160 \leq E_{lab} < 200$	$31.304 - 0.145E_{lab}$	$1.647 - 0.005(E_{lab} - 5)$	0.288	$12.7 - 0.025(E_{lab} - 160)$	$4.8 - 0.025(E_{lab} - 160)$
$200 \leq E_{lab} < 215$	"	"	"	11.7	3.8
$215 \leq E_{lab} < 220$	0	"	"	"	"
$220 \leq E_{lab} \leq 500$	"	0.1	"	$11.7 + 0.02(E_{lab} - 220)$	$3.8 + 0.02(E_{lab} - 220)$

TABLE II: Energy-dependent optical-model parameters of the potential n-^{12}C for $E_{lab} \geq$160MeV. At lower energies, the parametrization is the same as for ^{9}Be on Table I.

INFN Angela Bonaccorso
Istituto Nazionale di Fisica Nucleare

A.B & R. J. Charity, PRC89, 024619 (2014)

n+^{9}Be

Resonances described by $\delta V(r) = 16\alpha \frac{e^{2(r-R^R)/a^R}}{(1+e^{(r-R^R)/a^R})^4}$. consistent with dispersive contribution

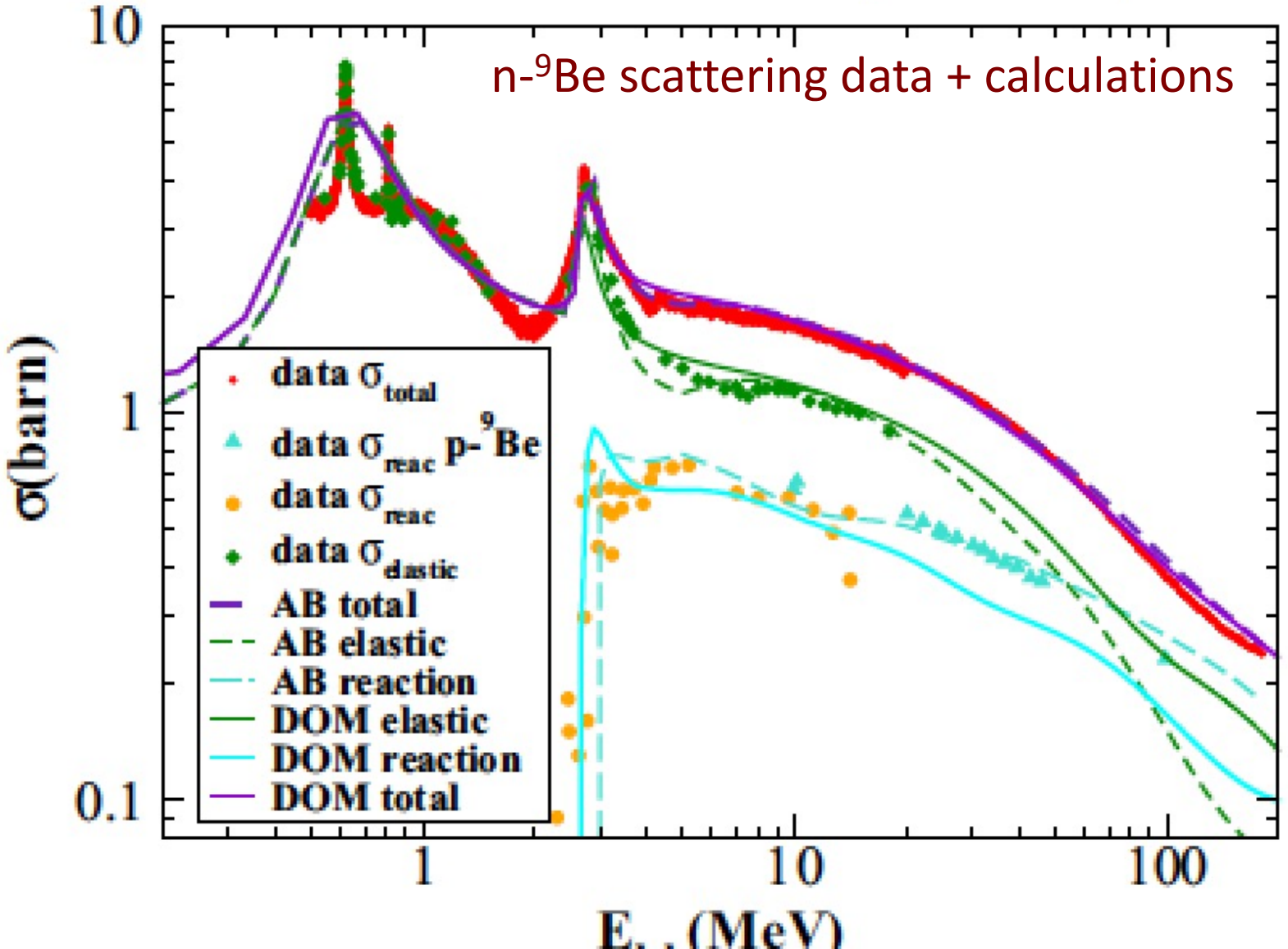

F.Flavigny et al., PRL 108, 252501 (2012)

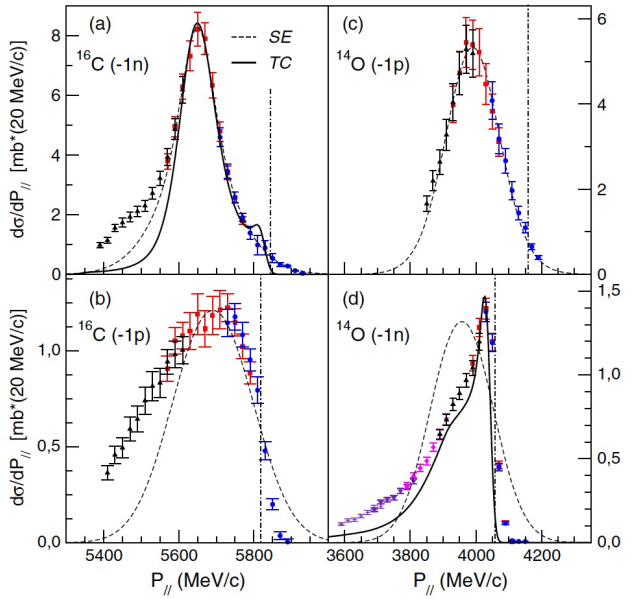

^{12}C

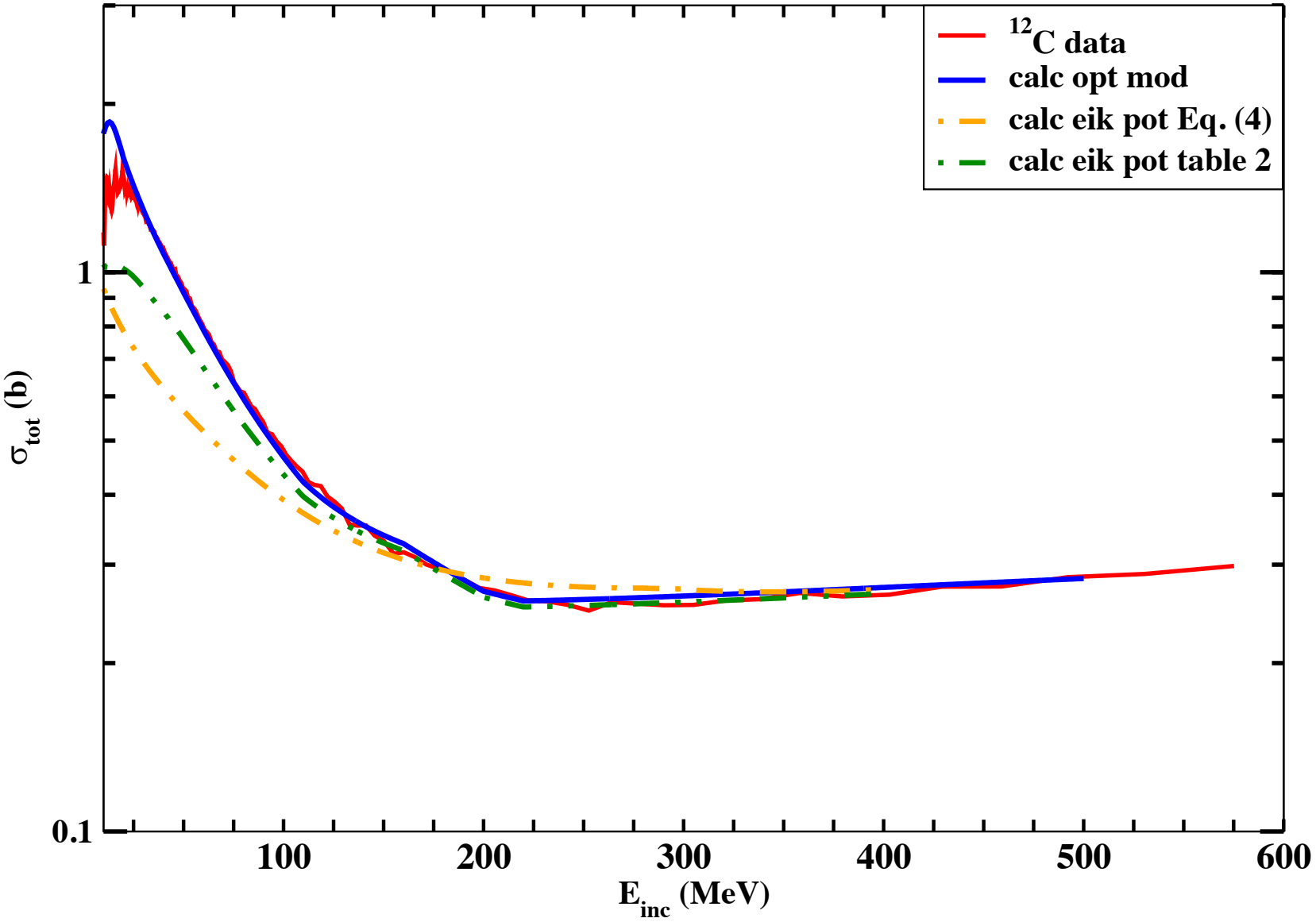
12C data
calc opt mod
calc eik pot Eq. (4)
calc eik pot table 2
σtot (b)
1
0.1
100
200
300
400
500
600
Einc (MeV)

Total experimental and calculated cross sections. Lower blue symbols for ^{9}Be, upper red symbols for ^{12}C. The optical model calculations are given by the orange and cyan dashed lines, respectively. The solid green line is a calculation made with a DOM potential obtained for ^{12}C and applied to ^{9}Be. DOM calculations (LHS) curtesy of Mack Atkinson (LLNL)

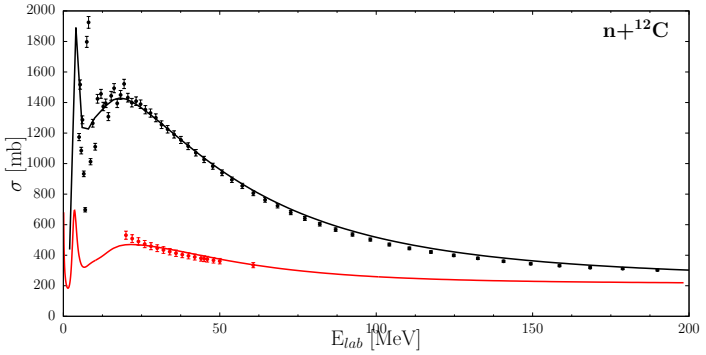

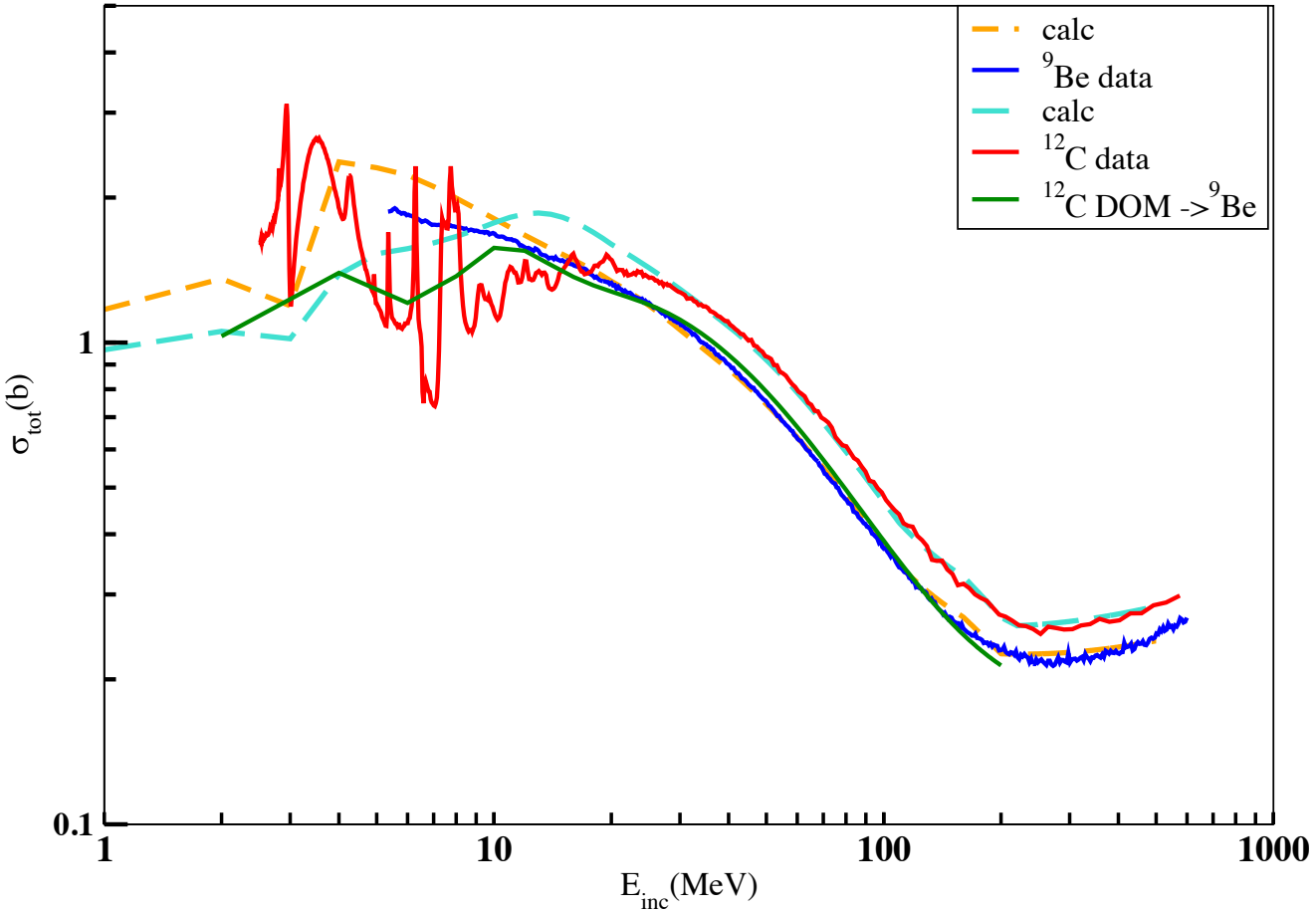

n+ ^{12}C , ^{12}C+^{12}C….
dominance of surface absorption

VGFM(Wiringa)
https://www.phy.anl.gov/theory/research/density/

NCSM

Ab initio no-core shell-model description of $^{10–14}$C isotopes

Priyanka Choudhary, Praveen C. Srivastava, Michael Gennari, and Petr Navrátil
Phys. Rev. C **107**, 014309 – Published 20 January 2023

Thanks to Petr Navratil and Michael Gennari for providing the numerical densities

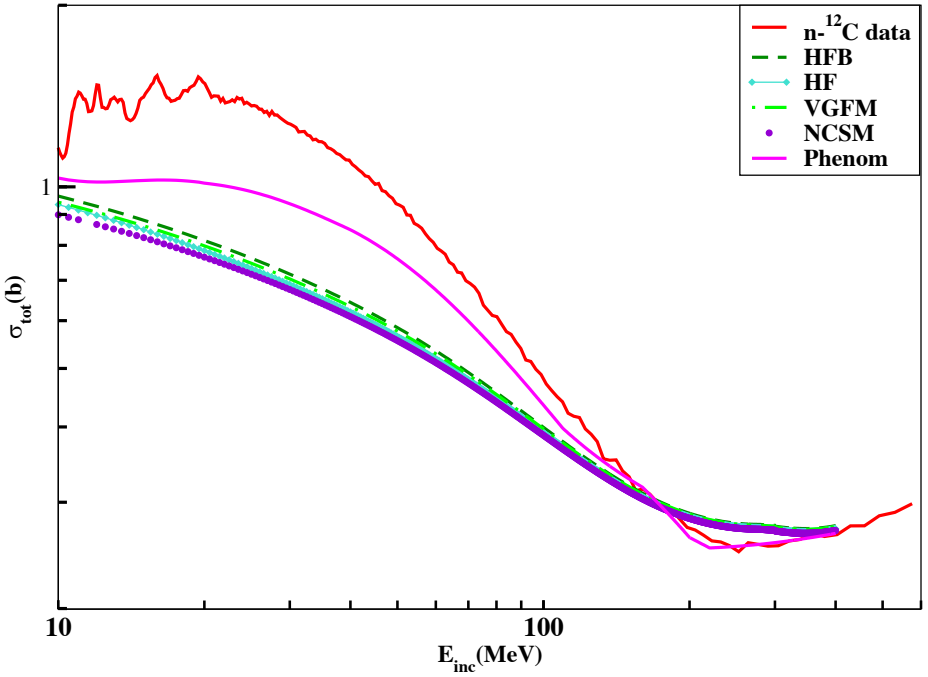

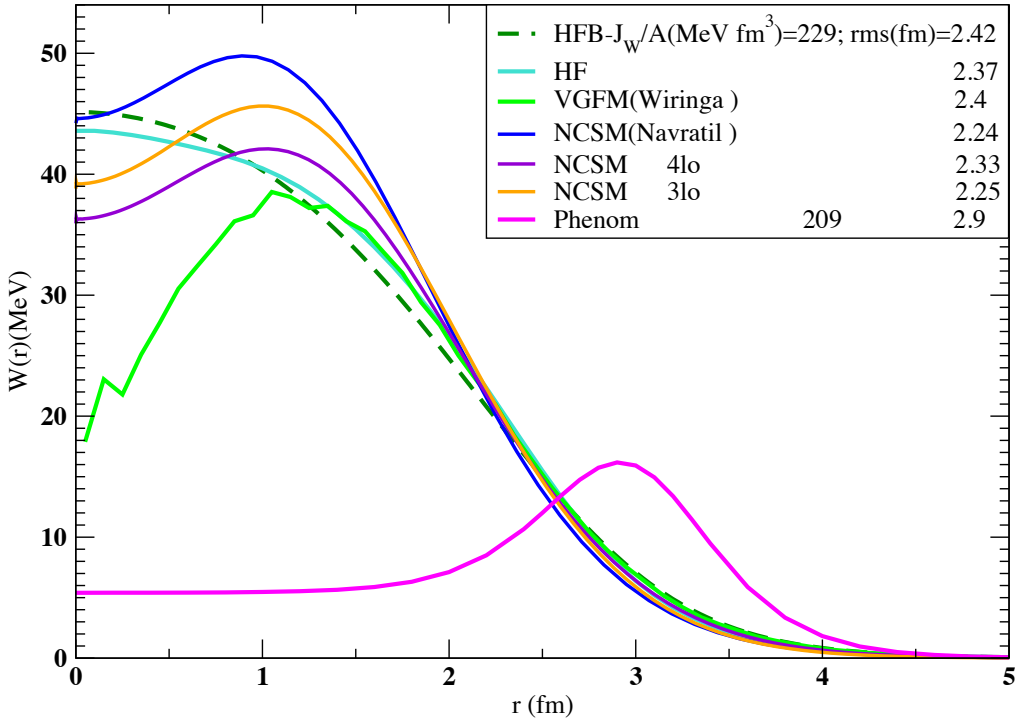

d.f. vs s.f. for NN potentials

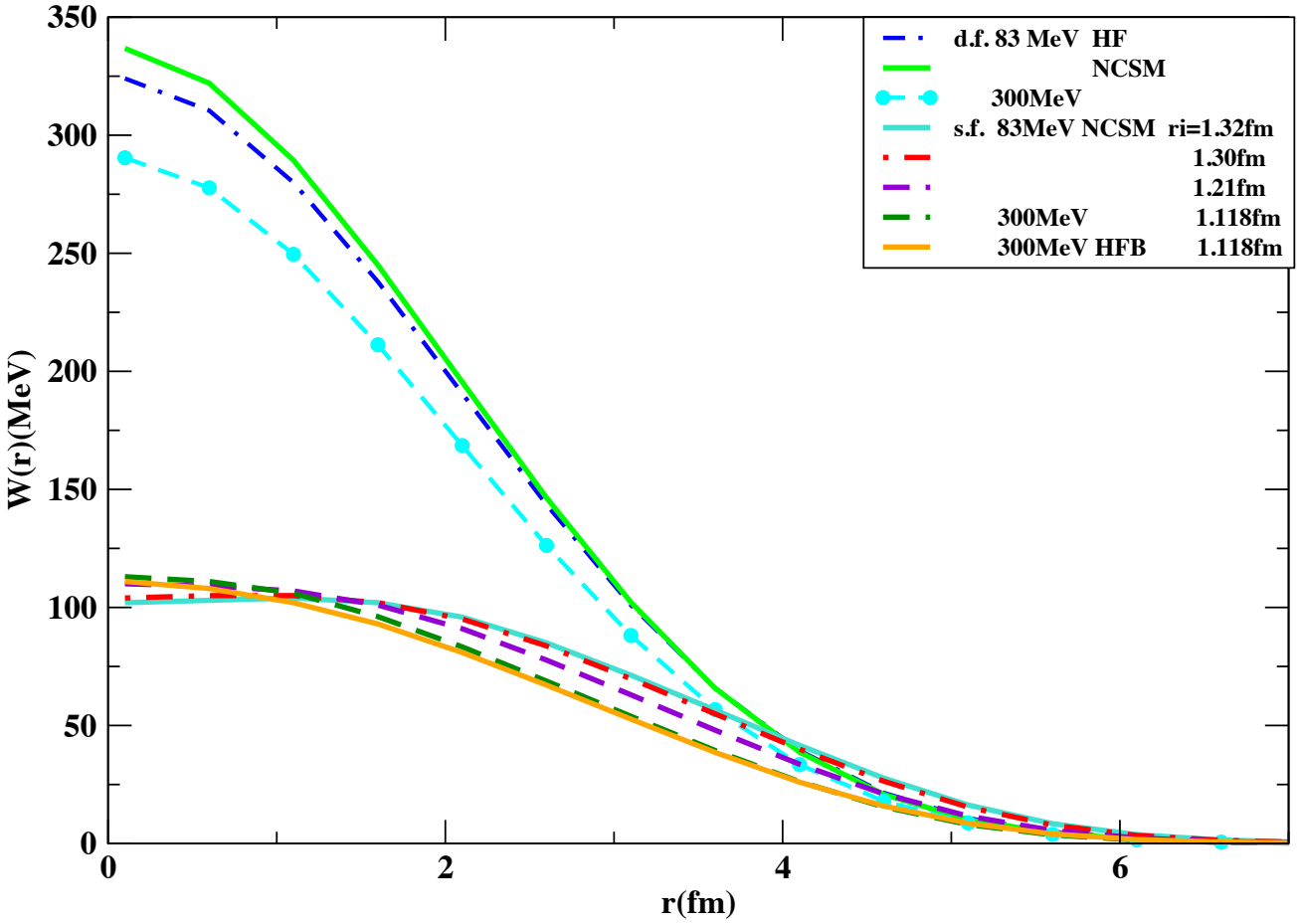

A possible, interesting evolution

- d.f. with *ab-initio* nN potential?
- See Finelli- Vorabbi-Giusti *arXiv:2212.00417v1*
- Densities from (NCSM), and/or Barbieri (Green-function)

Data from Takechi et al. cf slide 5, Kox
In d.f. $\sigma_{np,pp}$ from De Conti&Bertulani PRC81.064603 (2010).

E_{lab} (MeV)	$r_i(^9Be)$ (fm)	$r_i(^{12}C)$ (fm)
$30 \leq E_{lab} \leq 160$	$1.4 - 0.0015E_{lab}$	$1.32 - 0.0013E_{lab}$
$E_{lab} > 160$	1.15	1.118

TABLE III: Energy-dependent optical-model parameter r_i for the (AB) potential for n+^{9}Be and n+^{12}C

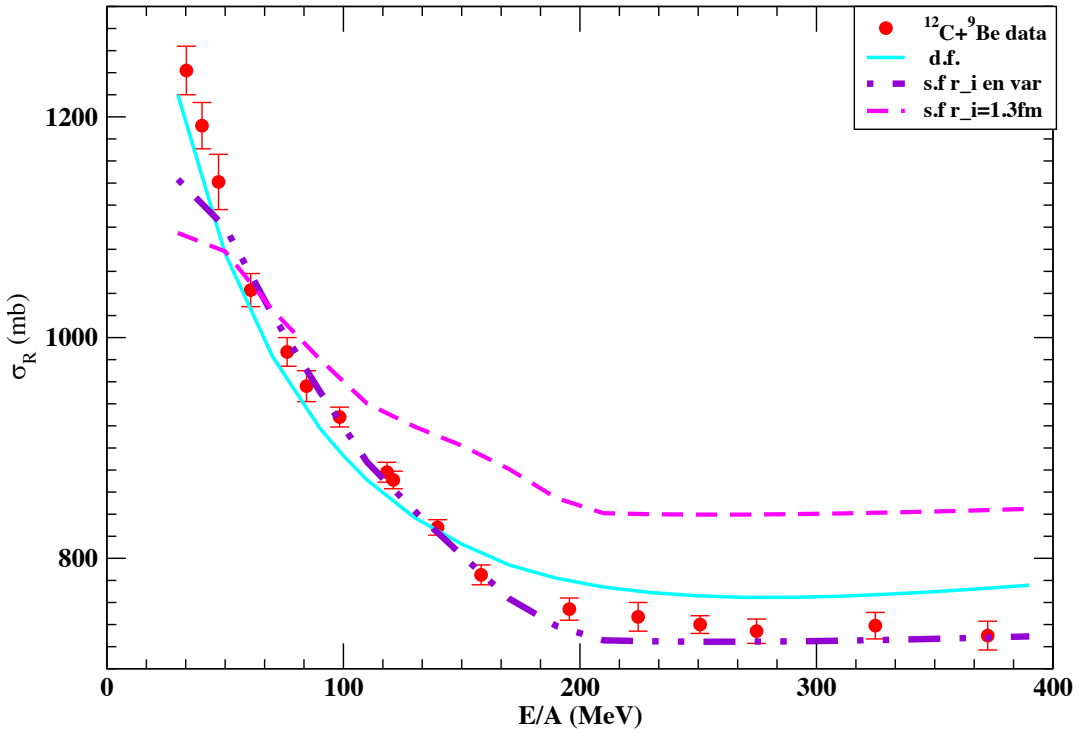

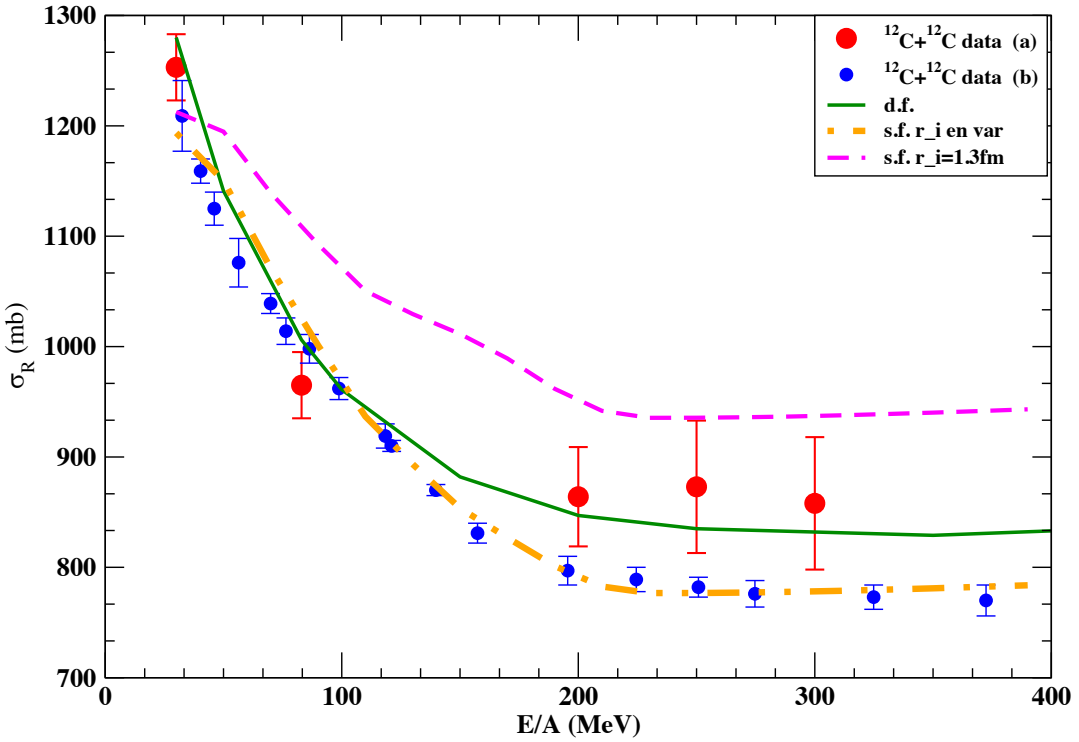

$^{12}C+^{12}C$

E_{inc} (MeV)	model	r_s (fm)	J_W/A_PA_T (MeVfm^3)	r.m.s (fm)	σ_{NCSM} (mb)	r.m.s (mb)	σ_{HF} (mb)	r.m.s	σ_{HFB}
83	s.f.	1.2	184	3.72	994	3.75	1008	3.78	1025
	d.f.	1.22	279	3.29	957	3.36	995	3.43	1027
300	s.f.	1.18	151	3.57	760	3.60	768	3.64	780
	d.f.	1.11	241	3.29	791	3.36	815	3.43	842

^{12} Ne+^{12}C

E_{inc}(MeV)	model	r_s(fm)	σ_{theo} (mb)	σ_{exp} (mb)
30	s.f.	1.35(1.33)	1478(1456)	1550 ±75
	d.f.	1.37	1560	
100	s.f.	1.27(1.23)	1327(1211)	1161 ± 80
	d.f.	1.21	1206	
200	s.f.	1.21(1.11)	1193(1012)	1123 ± 80
	d.f.	1.15	1079	
300	s.f.	1.21(1.12)	1181(1001)	1168 ± 100
	d.f.	1.13	1062	

280A.MeV

Nucleus	model	r_s(fm]	σ_{theo} (mb)	σ_{exp} (mb)	$r.m.s.$(fm)
^{42}Ca	s.f.	1.23(1.14)	1598 (1388)	1463(13)(6)	3.38
	d.f.	1.16	1460		
^{43}Ca	s.f.	1.22(1.14)	1614(1402)	1476(11)(6)	3.40
	d.f.	1.17	1476		
^{44}Ca	s.f.	1.23(1.15)	1630 (1417)	1503(12)(6)	3.42
	d.f.	1.16	1490		
^{46}Ca	s.f.	1.24(1.15)	1683(1466)	1505(8)(6)	3.50
	d.f.	1.17	1543		
^{48}Ca	s.f.	1.23(1.16)	1714(1495)	1498(17)(6)	3.50
	d.f.	1.18	1573		

Conclusions

- We have derived excellent n+^{9}Be, n+^{12}C phenomenological optical potentials up to 500MeV, cross checked vs DOM.
- Also excellent single folding P (Core)-T OP validated for ^{12}C + ^{12}C , ^{12}C+^{9}Be.
- Dominance of surface absorption (r_i decreases with energy).
- s.f. less ambigous than d.f. (needs to fix a smaller n of parameters).
- Evolution of d.f. via nN *ab-initio?*

$^{9}C+^{9}Be$

ELSEVIER

Nuclear Physics A 706 (2002) 322–334

NUCLEAR PHYSICS A

www.elsevier.com/locate/npe

Optical potentials of halo and weakly bound nuclei

A. Bonaccorso [a,*], F. Carstoiu [b]

Few-Body Syst (2016) 57:331–336
DOI 10.1007/s00601-016-1082-4

CrossMark

A. Bonaccorso · F. Carstoiu · R. J. Charity · R. Kumar
G. Salvioni

Differences Between a Single- and a Double-Folding Nucleus-^{9}Be Optical Potential

PHYSICAL REVIEW C **94**, 034604 (2016)

Imaginary part of the ^{9}C -^{9}Be single-folded optical potential

A. Bonaccorso,[1,*] F. Carstoiu,[2] and R. J. Charity[3]

M. Fukuda et al., private communication; D. Nishimura et al.,Osaka University Laboratory of Nuclear Studies (OULNS) Annual Report 2006, p. 37.

E_{lab} (MeV/nucleon)	σ_{exp} (mb)	$\sigma_{d.fold}^{VMC}$ (mb)	$\sigma_{d.fold}^{HF}$ (mb)	$\sigma_{s.fold}$ (mb)	$\sigma_{s.fold}^{+surf}$ (mb)	σ_{JLM}^{bare} (mb)	σ_{JLM}^{ren} (mb)	N_{JLM}	W_{surf} (MeV)	R_s (fm)	R_s^{fit} (fm)	a^{fit} (fm)	r_s (fm)
20		1267	1409	1078	1565	1338	1538	1.65	0.8	6.12	6.25	1.01	1.47
38		1086	1191	1112	1341	1250	1324	1.20	0.5	5.95	5.99	0.97	1.44
40.9	1216 ± 57	1064	1166	1117	1291	1235	1215	0.95	0.4	5.95	5.99	0.98	1.44
43		1050	1148	1103	1275	1221	1260	1.10	0.4	5.95	5.99	0.99	1.44
43.6	1269 ± 22	1046	1144	1106	1235	1219	1257	1.10	0.3	5.82	5.70	0.80	1.40
59		960	1042	1047	1124	1130	1111	0.95	0.2	5.70	5.64	0.82	1.36
61.1	1104 ± 20	950	1030	1045	1122	1119	1119	1.00	0.2	5.68	5.63	0.83	1.36
66		928	1006	1028	1066	1091	1028	0.85	0.1	5.60	5.55	0.80	1.35
67.4	1074 ± 32	923	999	1026	1056	1087	1087	1.00	0.08	5.60	5.53	0.80	1.35
68.3	1064 ± 16	919	995	1024	1052	1082	1063	0.95	0.075	5.55	5.49	0.80	1.33
83		867	934	948	979	1015	987	0.93	0.015	5.40	5.38	0.78	1.29
84.9	981 ± 15	861	928	979	983	1008	989	0.95	0.01	5.40	5.36	0.80	1.29
95		833	895	949	952	968	956	0.97	0.01	5.40	5.28	0.79	1.29
97.2	919 ± 24	827	888	949	951	963	923	0.90	0.005	5.35	5.28	0.80	1.28

Comparison with data, at low energy suggests the need to include the ^{9}C breakup channel explicitly

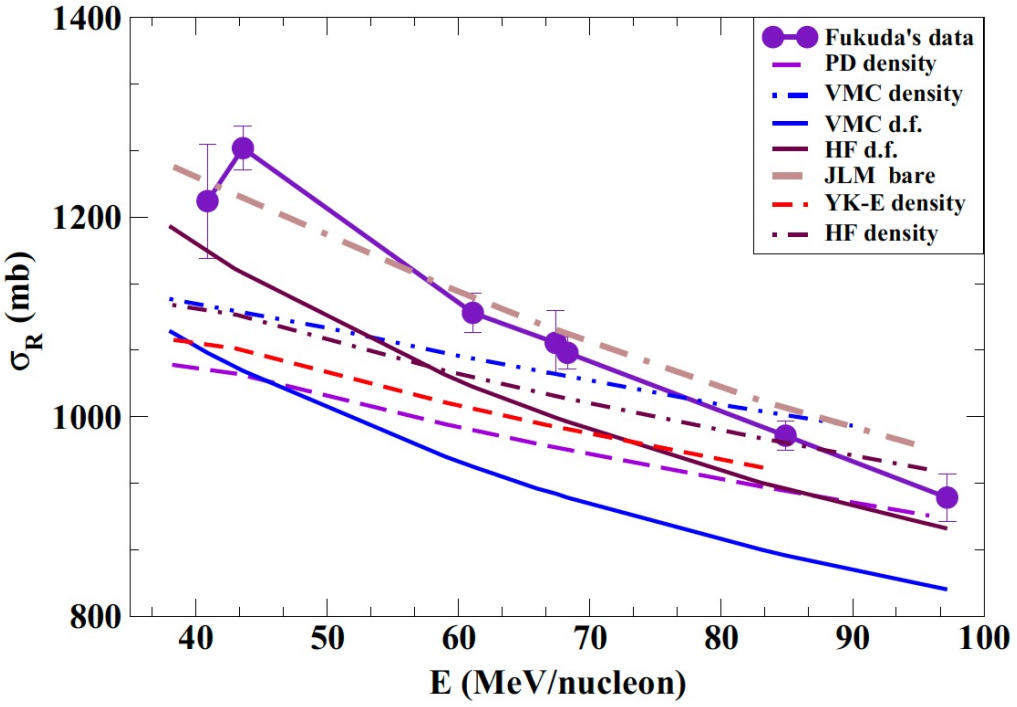

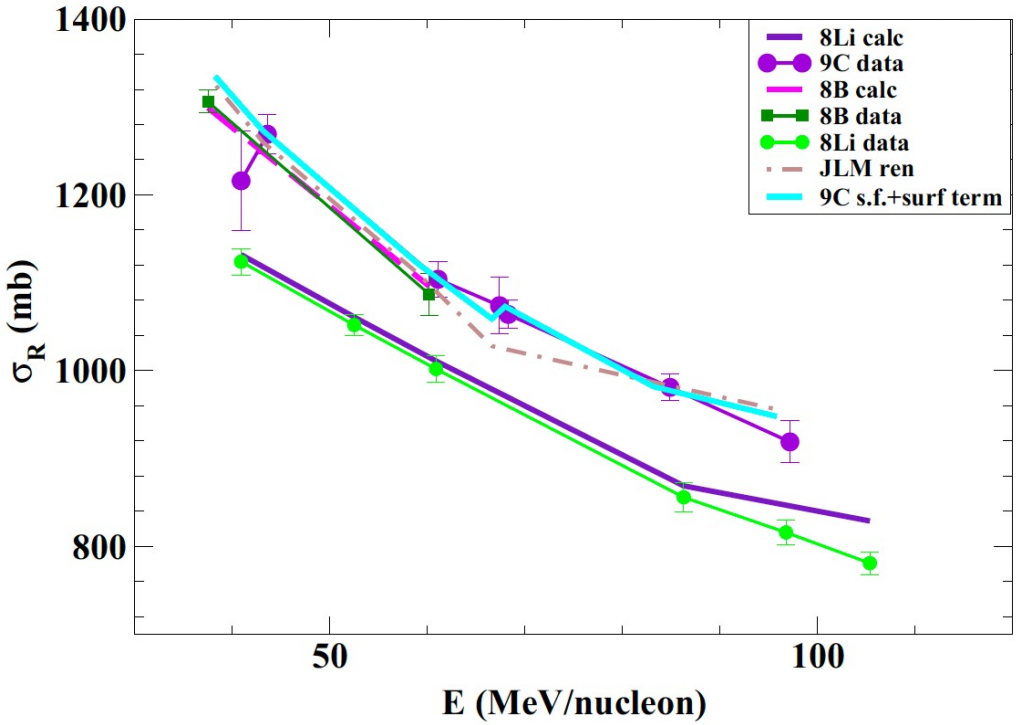

- The above definition of the profile function is equivalent to define a 3d imaginary potential of gaussian shape normalized to 1 whose depth is $-\frac{1}{2}\hbar v\sigma_{nn'}$

A Schematic Theory of Nuclear Cross Sections*

H. FESHBACH AND V. F. WEISSKOPF
Department of Physics and Laboratory for Nuclear Science and Engineering, Massachusetts Institute of Technology Cambridge, Massachusetts

(Received August 8, 1949)

neutrons are then

$$\sigma_r^{(l)} = (\pi/k^2)(2l+1)(1-|\eta|^2) \tag{7a}$$

$$\sigma_{el}^{(l)} = (\pi/k^2)(2l+1)|1+\eta|^2 \tag{7b}$$

$$\sigma_{tot}^{(l)} = (\pi/k^2)(2l+1)2(1+Re\eta). \tag{7c}$$

η_l can be adjusted so that (6) fulfills the boundary condition (5):

$$\eta_l = -\frac{xu_l'+iXu_l}{xv_l'+iXv_l},$$

where u_l and v_l are the values, u_l' and v_l' the derivatives in respect to x, of the functions (7) evaluated at $x=kR$. We define the phases δ and δ' by $v=|v|e^{i\delta}$ and $v'=|v'|e^{i\delta'}$ and use the Wronskian relation $|vv'|\sin(\delta_l'-\delta_l)=1$. We then get[c]

[b] This approach is similar to that of H. Bethe (Phys. Rev. **57**, 1125 (1940) to describe nuclear absorption.